July 2018

A New Control Framework For The Visual Environment Based On Low-Cost HDR Luminance Acquisition

Michael Kim
Lyles School of Civil Engineering, Purdue University; Center for High Performance Buildings, Ray W. Herrick Laboratories, Purdue University, kim2384@purdue.edu

Iason Konstantzos
Lyles School of Civil Engineering, Purdue University; Center for High Performance Buildings, Ray W. Herrick Laboratories, Purdue University, ikonsta@purdue.edu

Athanasios Tzempelikos
Lyles School of Civil Engineering, Purdue University; Center for High Performance Buildings, Ray W. Herrick Laboratories, Purdue University, ttzempel@purdue.edu

Follow this and additional works at: https://docs.lib.purdue.edu/ihpbc

A New Control Framework for the Visual Environment Based on Low-Cost HDR Luminance Acquisition

Michael KIM[1,2], Iason KONSTANTZOS[1,2]*, Athanasios TZEMPELIKOS[1,2]

[1]Lyles School of Civil Engineering, Purdue University

[2]Center for High Performance Buildings, Ray W. Herrick Laboratories, Purdue University

* Corresponding Author

ABSTRACT

This study introduces a new control framework, based on a low-cost programmable luminance acquisition (HDR) sensor placed on the interior surface of the window. The new sensor, photometrically and geometrically calibrated, can capture luminance and geometry details of potential glare sources within its entire visual span in real time, while also providing feedback about transmitted illuminance. Real-time processing of the sensor data enables an alternate, low-cost glare sensing system that can be directly used in daylighting controls and building automation systems. This novel framework is the first proposed solution to address direct and reflective glare in a straightforward and efficient way and therefore it is a significant step towards improving the visual environment in perimeter building zones.

1. INTRODUCTION

Discomfort glare is a main concern, especially when it comes to private and open plan offices of modern commercial buildings. Placing workstations close to the window, combined with the use of large facades often creates indoor environmental conditions that can compromise the satisfaction of the building's occupants and limit daylight harvesting potential while also having significant implications in terms of well-being and productivity. Nevertheless, daylighting is essential in modern buildings, benefitting circadian rhythms, and saving energy by minimizing the use of electric lighting. Therefore, it is a priority to focus on methods of efficient glare mitigation that will maximize daylight harvesting potential without compromising the indoor environment with instances of discomfort. In that scope, a variety of studies focused on glare investigation, including experimental studies with human subjects (Wienold and Christoferssen, 2006, Hirning et al. 2014; Jakubiec and Reinhart 2012; Karlsen et al. 2015; Konis 2013; Sadeghi et al. 2016, Konstantzos and Tzempelikos, 2017, Van den Wymelenberg et al., 2010; Van den Wymelenberg and Inanici, 2014), experiments with dynamic shading (Konstantzos et al. 2015a), and modeling studies using existing and new glare indices (Atzeri et al. 2014; Chan et al., 2015, Wienold 2009). Tzempelikos (2017) commented on the dynamic variation of daylighting and the need for further research, including emphasis on subjective factors, as hidden variables with quantified uncertainty to ultimately lead to more systematic, holistic and robust performance metrics. Although the most efficient way to ensure maintaining comfortable conditions in the interior is through efficient design and seating layouts (Jakubiec and Reinhart, 2012; Jakubiec and Reinhart, 2015; Konis, 2013; Konis, 2014; Konstantzos et al. 2018), in cases of existing buildings or poor flexibility, shading controls are an effective solution. Their relatively low cost, their variability in terms of optical and solar characteristics and their aesthetic flexibility are advantages that have placed roller shades among the most widely used shading approaches in the US. Several studies have been published over the past years related to roller shades, investigating different aspects; the impact of their properties on outside view (Konstantzos et al., 2015) and on glare mitigation (Chan et al,. 2015, Konstantzos and Tzempelikos, 2017), and efficient control algorithms (Park et al. 2011; Shen and Tzempelikos 2012; Singh et al. 2015; Tzempelikos and Athienitis 2007; Shen and Tzempelikos, 2017; Yao 2014). Recent state-of-the art control approaches can effectively minimize glare occurrences when paired with optimal fabric properties selection (Konstantzos et al. 2015b; Shen and Tzempelikos, 2017). Their simplest forms are based on tracking the solar path, and can increase in complexity, either by adding extra window feedback sensors or by implementing extra constraints in terms of the light levels on the occupant's position (Shen and Tzempelikos, 2017).

However, even the most advanced algorithms, applied with fabrics of "optimal" properties, fail to address reflective glare induced by exterior obstructions, such as reflective facades of adjacent buildings. This is a situation that can

occur frequently in scarce urban environments, where curtain wall-based buildings are located close to each other (Suk et al., 2016). During these instances, the sun gets reflected on a specular way on the buildings' surfaces, creating sources of extreme luminance perceived from the interior of adjacent buildings. When this happens, existing control systems, based either on solar path tracking or with added support of illuminance sensors on the window, are not able to detect the bright sources, partly because of solar geometry suggesting the absence of sun during these times, and also due to the fact that extreme luminance sources do not always contribute significantly to the vertical illuminance as it is perceived by the window sensors. Consequently, the control system might leave the shades open, creating conditions of extreme discomfort or even disability glare in the interior.

This paper proposes a new framework to address the above issue, introducing an extra layer of glare detection and protection based on a programmable luminance acquisition sensing device on the window. The new low-cost sensor operates on a 5-minutes interval capturing the exterior conditions and detects potential sources of discomfort with respect to their luminance, size and position. Then, a decision-making approach identifies the potential of these sources to cause discomfort to the interior, and accordingly operates the shading to a level where these sources will be blocked from the interior observer's position. The study describes the methodology of photometric and geometric calibration of the lens, goes through the principles of a control algorithm, and presents an implementation, comparing the new framework with current state-of-the-art.

2. METHODOLOGY

2.1 A new low cost camera sensor
Integrated board computers have gained popularity over the past few years due to their very low price, small size and ability to adopt to different problems through both hardware using expansion boards or customized codes. The computer used in the study runs a UNIX-based operating system and can run Python-based scripts that have been created to cover every aspect of the methodology discussed in this study, presented in detail in Section 2.2.

The study uses a camera on board chipset based on a CMOS sensor (Figure 1 left), offering a resolution of 8 megapixels for still imagery. Typically, the camera is paired with a fixed focus lens of 3.4mm focal length. However, as the objective of the study required maximizing the field of view, the standard lens was replaced by a fisheye lens, with an aperture of f/1.8 and a focal length of 1.02mm. In order to mount the lens to the camera, a custom box was designed and 3D-printed, as well as a stand to attach the system on the window (Figure 1 right).

Figure 1: Camera-on-board chipset (left) – Finalized window sensor with 3D-printed case and mount (right)

2.2 HDR Imaging - Photometric and Geometric calibration
As the objective of the newly developed sensorwas to obtain a detailed luminance map of the visual field, High Dynamic Range (HDR) imaging techniques were implemented, as discussed by Inanici (2006). This method is based on shooting photographs at different exposures for any given time step; merging them into HDR images; applying photometric and geometric calibration procedures and then running Evalglare (Wienold, 2017) in order to analyze them and identify potential glare sources, in terms of luminance, size and position relative to the line of sight; and calculate luminance and illuminance-based metrics, if needed. The process sequence can be seen in Figure 2. HDR

imaging with camera-on board chipsets and integrated board computers has been attempted before in literature (Goovaerts et al., 2017), but more focused on the photometric side and without details about the required geometry calibration.

In that scope, a script was created to schedule the camera to take a full set of exposures every five minutes, with shutter speeds ranging from 0.000028s to 0.0078s. Then, the freeware command-line tool HDRgen (Ward, 2005) has been utilized to merge the low dynamic range pictures to a high dynamic range image, implementing a response curve developed for the combination of lens and camera used in the experiment. The response curve is a function associating radiometric intensity to absolute values of luminance and is obtained using a calibration procedure; the latter is based on correcting the luminance value at a given point of relatively neutral spectral characteristics from the HDR image with the value obtained by a scientific-grade calibrated luminance spot meter, and then applying the correction factor to the rest of the image (Reinhart et al., 2017). Due to the fast aperture (f/1.8) of the used lens, an additional correction for vignetting needed to be implemented; vignetting is the radial decrease of luminance observed in fisheye lenses of fast apertures that can potentially compromise the accuracy of measurements. The process presented by Inanici (2006) was followed to develop a 5th degree polynomial correction function, which was then implemented in the image through RADIANCE (Ward, 1994). The above steps ensured an accurate luminance distribution in the resulting image. However, as detailed information about the position and size of glare sources is also required, the images needed to be additionally geometrically corrected. This required a detailed geometric calibration of the camera.
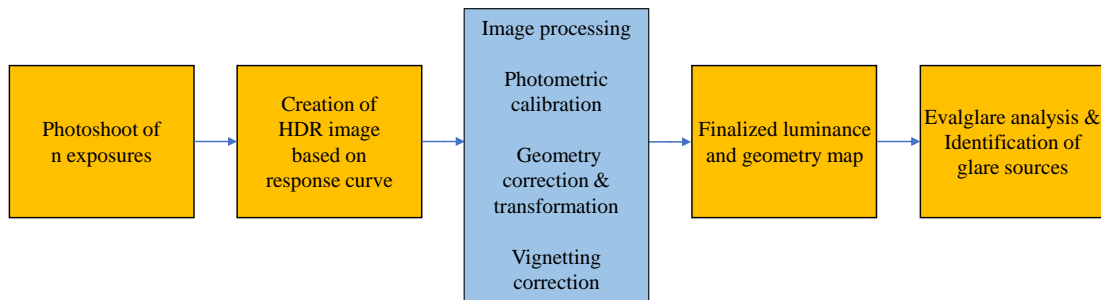
Figure 2: Flow chart of HDR imaging process

Geometric calibration is a process that estimates the camera projection that maps real-world scenes into image pixels. After a proper geometric calibration, it is possible to retrieve the position of an object relative to the camera through back-projection of the image pixels.

There are various distortion models for fisheye cameras that are mostly based on radial distortion, a function of pixel radius from the distortion center. In this study, a distortion model for omnidirectional camera proposed by Scaramuzza (2006) was used. The model estimates the 3-D directional vector emanating from the viewpoint as a function of pixel radius from the distortion center, as seen in Eq. (1).

$$\begin{bmatrix} X_c \\ Y_c \\ Z_c \end{bmatrix} = \lambda \begin{bmatrix} u \\ v \\ \mathrm{f}(\rho) = a_0 + a_2\rho^2 + a_3\rho^3 + a_4\rho^4 \end{bmatrix} \tag{1}$$

, where $[X_c, Y_c, Z_c]^\mathrm{T}$ is the 3-D vector corresponding to the image point, u and v are pixel distances from the distortion center in X and Y axis, λ is a scalar factor, ρ is the pixel radius from the distortion center ($\rho = \sqrt{u^2 + v^2}$), and $[a_0, a_2, a_3, a_4]$ are coefficients for the Z-component retrieval (Figure 3).

The estimated function f from the calibration enables us to inverse-project pixels into θ, the angle between the optical axis and 3-D vector to the real-world scene. This made it possible to retrieve the angle θ from any pixel of an image, as observed in Figure 5 (left) and Equation 2.

$$\rho = \mathrm{projection}(\theta) \leftrightarrow \theta = \mathrm{projection}^{-1}(\rho) = \arctan\left(\rho / \mathrm{f}(\rho)\right) \tag{2}$$

The estimated projection curve can be used for radial transformation of HDR images which is essential for accurate geometry mapping. Evalglare is compatible only with HDR images of standard projections, such as equidistant (a projection that θ is proportional to ρ). A sixth-order polynomial fitting was performed to transform the fisheye projection into equidistant projection, using Radiance pcomb command (Figure 4), according to the methodology described by Geisler – Moroder et al. (2016).
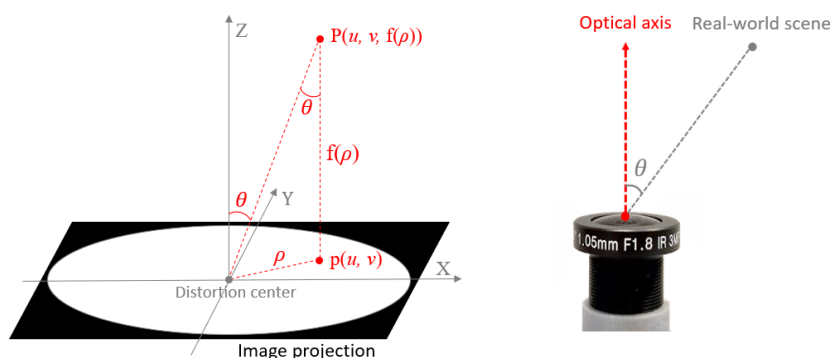
Figure 3: Illustration of fisheye camera projection model used

In order to effectively validate the HDR imaging methodology, including photometric and geometric aspects, a validation in terms of vertical illuminance was selected. As vertical illuminance is a function of the contribution of the luminance, solid angle and position of every pixel, comparing the resulting vertical illuminance values with the ones obtained by a calibrated photometer is an effective way to evaluate the methodology. As seen in Figure 6 (right), a satisfactory fit is observed.

It has to be noted that the values seen in Figure 5 were obtained at conditions when the sun was not in the field of view; as discussed in literature (Konstantzos et al., 2015a), HDR imaging involves challenges in cases of the sun being in the field of view and observed from the interior of the room. This is a result of the still limited dynamic range of HDR imaging, when it needs to simultaneously capture ranges at the order of 10-100cd/m^2 within the room and ranges at the order of 10^9 cd/m^2 that can occur in the solar disc. This issue creates a maximum value of observed luminance in the images obtained by our system at the level of 10^6 cd/m^2, leading to severe underestimation of luminance values over that peak value, and also vertical illuminance calculations with the sun in the field of view. The authors have addressed this issue in the past with using ND filters (Konstantzos and Tzempelikos, 2017; Strumpfel et al., 2006), this technique however was decided not to be used in this particular application because of the high exposure times it involved. Different options are explored to address this issue in near future, however the problem does not affect the operation of the proposed sensor, since the operating thresholds that will trigger shade movements are varying well below the measuring capacity of 10^6 cd/m^2, as explained in section 2.3.
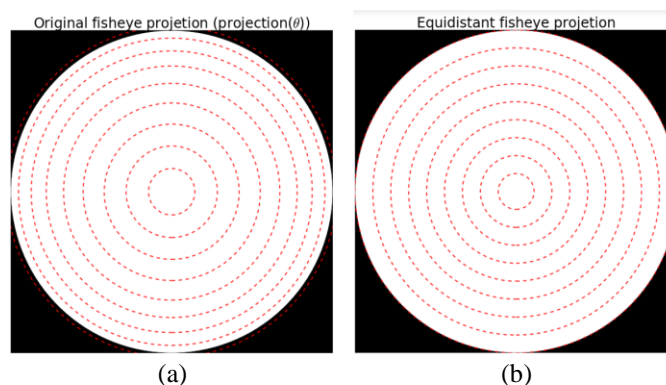

(a)   (b)

Figure 4: (a) Original fisheye projection (b) equidistant projection.
Each circle corresponds to equal θ with 10-degree increment. (from 10 degrees to 90 degrees)
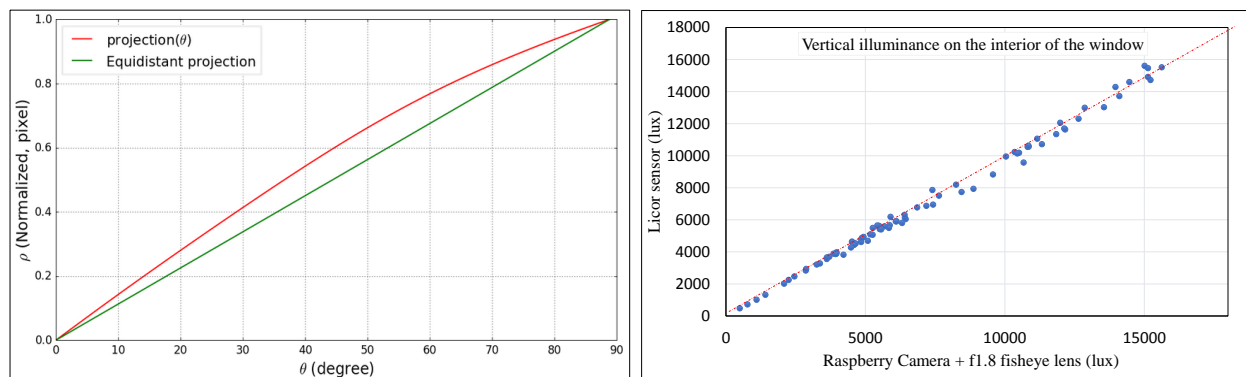
Figure 5: Estimated fisheye camera projection curve (left) – Vertical Illuminance validation (right)

2.3 Implementation of HDR imaging in a novel control framework

In order to test and validate the operation of the new sensor, it was attached to the inside glazing surface of a 3,3m x 3.7m x 3.2m private office, located on the first floor of the Center for High Performance Buildings at Purdue University. The room had a South façade (54% window – to – wall ratio) with a relatively unobstructed view for a distance of 50m. The room was equipped with a high-performance glazing system (70% visible transmittance), motorized shading, based on a fabric of 2.18% openness factor and 2.53% visible transmittance and electric lighting, assisting the daylit operation with dimming. The occupant's position was assumed at a distance of 1m from the window, facing the window at a typical seating height of 1.20m, to approximate a worst-case scenario in terms of glare perception. At this position, a secondary camera (identical to the window sensor) was placed in order to observe the occupant's field of view (Figure 10 left). To obtain additional values of environmental variables of interest, such as illuminance transmitted from the window and total vertical illuminance at the observer's eye height, light sensors were used connected to a data acquisition system, along with a handheld illuminance meter for assistive measurements. The room was handled by a Building Management System (BMS) which gives the ability to monitor, control and modify all building systems, including the motorized shades. In order to establish communication between the BMS and the window sensor, the MODBUS TCP protocol was used, in a framework described in Figure 6.
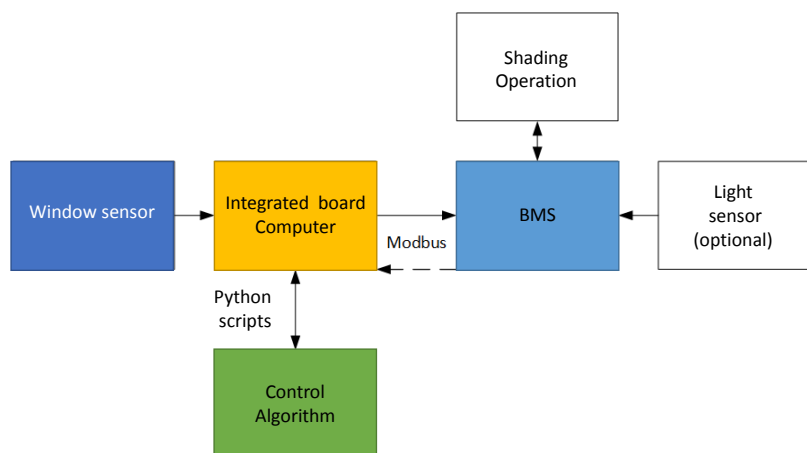

Figure 6: Framework of window sensor and dynamic shading operation

The newly developed sensor was placed on the window, at the occupant's eyes height. The BMS was configured to apply a conventional control, based on:

- Preventing direct light hitting the occupant's work plane at a distance of 1m
- Opening the shades if the outside conditions are dark due to overcast sky (transmitted illuminance <10,000 lux)
- Lowering the shades if the outside conditions are extremely bright, even if no direct sunlight hits the workspace (transmitted illuminance > 30,000 lux)

The new sensor is proposed to be implemented as an additional layer of protection, to lower the shades when a bright instance over a specific threshold was detected in the exterior. Due to the lack of a validated luminance border of visual discomfort for that particular case of glare (i.e., due to exterior bright small-sized sources) in literature, defining operating thresholds for such purposes is a challenging process involving experiments with human subjects and is part of the current work of the authors; however, in this paper a proof of concept of the method is presented, based on preliminary observations, placing the operating threshold at the level of 30,000 cd/m^2.

In order to calculate the shading level protecting the interior from the reflected sources, the profile angle is used. It is computationally inefficient to iterate over every glare source pixel to find the minimum profile angle of entire glare sources in the scene. Thus, a simple method using only the pixel range of glare sources is used. For this method, the Evalglare source code was modified to output the pixel range of each glare source.
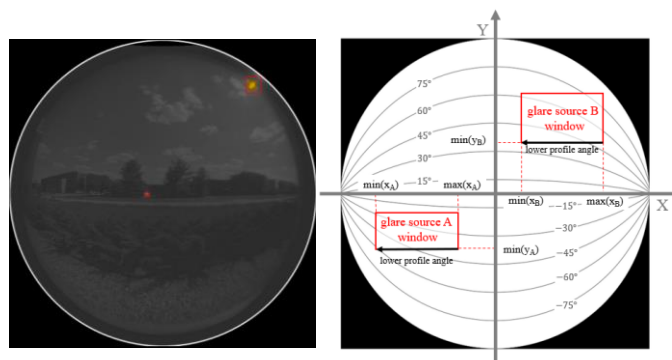

Figure 7: Glare source detection and pixel frame representation by modified Evalglare analysis (left)
Curves with equal profile angle in equidistant fisheye projection (right)
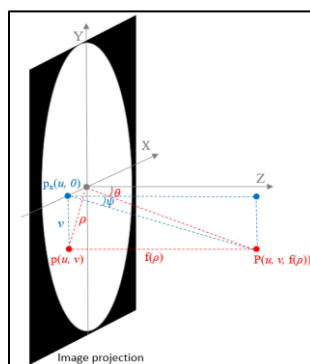

Figure 8: Profile angle from image projection

As seen in Figure 7(left), the pixels range of each glare source can be identified from the Evalglare output. However, simply using the lowest pixel of the glare source may fail to capture the actual lowest profile angle due to the high distortion of fisheye image. The bottom (fictitious) horizontal line of the glare source window with lowest Y-axis pixel position in Figure 7(right) is not actually horizontal in real-world scene. To have a conservative profile angle for glare protection, the X-axis pixel that corresponds to the lowest profile angle is selected. Determining the X-axis pixel differs for the lower and upper half of the fisheye projection; for the lower half of the image, the profile angle decreases as X-axis pixel is further from the Y-axis, and for upper half, the opposite happens. Choosing a pixel p(u,v) by this method will always result to a profile angle that is lower or equal to the actual lowest profile angle of a glare source, without requiring any heavy computation.

The final profile angle calculation is performed by back-projection of the chosen pixel into 3-D Cartesian coordinates as illustrated in Figure 8. The profile angle can be calculated by Equation 3.

$$\psi = \arctan\left({}^{v}\!/_{f(\rho)} \right) \tag{3}$$

, where ψ is the profile angle. The lowest profile angles are calculated for every glare source detected by Evalglare and choose the minimum of them for the glare protection.
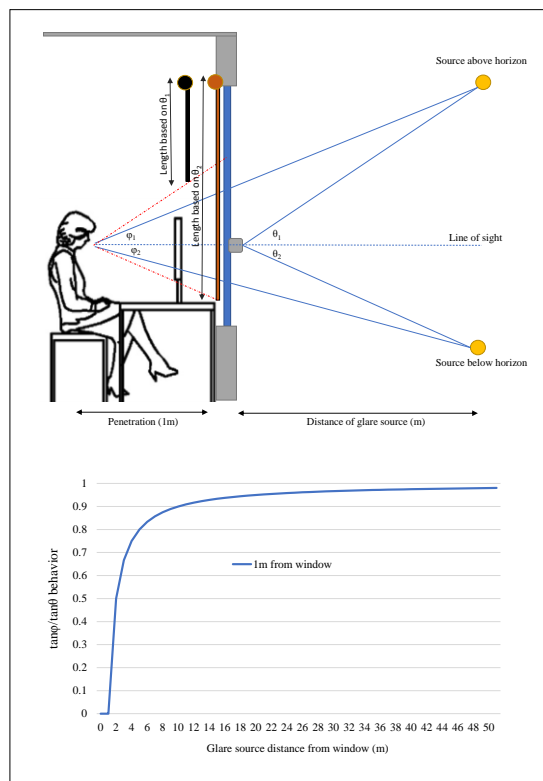

Figure 9: Angular differences issues; red dashed lines show the deviation inside, defining shading length decisions (top), fraction of the tangents of angles φ and θ depending on distance of glare source from the window (bottom)

This approach involves limitations: the visual field of an occupant located inside can be substantially different from the visual field perceived at the window camera in two different levels; (i) parts of the window sensor's visual field are not visible from the inside due to the window extents and (ii) a potential glare source visible by both can be observed in different angles from the occupant and from the window sensor. While (i) is a limitation that will always make the control more conservative, potentially blocking sources that are not visible, (ii) can be more complicated, having different results depending on whether the discomfort source is above or below the horizon. As seen in Figure 9 (top), if the source is above the horizon, the shade targets a position defined by profile angle θ_1, stopping at a level higher than the one required to protect the occupant. In contrast, for sources below the horizon, the shade position will be defined by angle θ_2, closing the shade slightly more than required, limiting the daylight harvesting potential.

This problem is fundamentally non-solvable without an approximation of the distance of the source from the window. However, in most occurrences of reflective glare from buildings, the trigger buildings are located at a significant distance from the affected ones. Figure 9 (bottom) shows how the angular difference gets minimized with distance of the glare source, minimizing the impact of the error for distances over 10m. Therefore, to comply with this limitation, the validation of the framework was performed for distances of over 12m from the window. In order to make the experimental procedure more flexible, reflections were induced by using highly reflective cardboards (0.42m x 0.40m), mounted on tilted tripods outside, as seen in Figure 10 (center and right).

The proposed control logic can be seen in Figure 11; every α minutes, a photoshoot sequence is scheduled. The 9 LDR images are being merged into HDR and processed to implement photometric and geometric transformations, the modified Evalglare algorithm is being used to detect glare sources and the profile angle of the lowest source is calculated. Then, the controller compares with the current shade position and, if the latter is higher, it will trigger the shades to be lowered to the new position.

Figure 10: Dual camera setup (left), Reflector mount (center) – Reflectors as seen from the observer position (right)
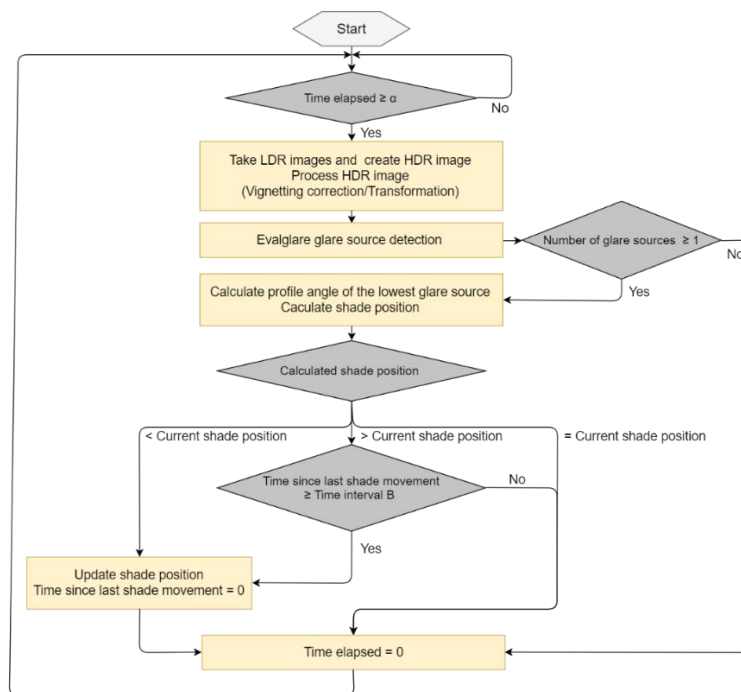

Figure 11: Control logic of the proposed framework

3. RESULTS - DISCUSSION

The new framework was tested in May 2018. Due to the limitation of having a South façade, the sun appeared very high in the sky, making the baseline controller assume fully open shades. This however gave the flexibility of testing different positions of reflected sources that would lead to discomfort if the shades were controlled using the conventional solar path tracking control of the BMS.

Figure 12 shows an example case with four detected glare sources; two induced by the reflectors and two due to the solar disc visible towards the edge of the visual field. The algorithm selects the lowest of the four sources, applies the methodology described in section 2.3 to calculate the minimum profile angle, and operates the shading in a way that blocks the lowest glare source from the occupant seated at the height of the window sensor. The reflectors were put in randomized positions at distances ranging from 12m to 40m away from the façade, in order to eliminate the angular difference effect between observer and window – sensor, as discussed in Section 2.3. However, the minimum distance of 12m, combined with the limited height of the reflectors (up to 3.5m, mounted on a ladder) kept the resulting minimum profile angles at a narrow margin, ranging from -7.10° (lowest) to 2° (highest). Nevertheless, this narrow range was adequate to help explore the efficiency of the framework. Figure 13 shows 10 different reflectors placements and how the shading positions triggered by the conventional solar path tracking algorithm of the BMS compare with the ones triggered by the new framework. Figure 13 also presents the minimum triggering profile angles and the

impact on maintaining the observer's vertical illuminance within acceptable standards of comfort (Konstantzos and Tzempelikos, 2017).

Figure 12: Framework operation example: (a) window sensor false color image with luminance mapping, (b) sources detection, (c) indoor view of window with conventional control (d) indoor view of window with control based on new framework

Figure 13: Selection of measurements; blue color shows the profile angle of lowest detected glare source, and green and red show opened shade portion and vertical illuminance at the occupant's eye level for the new framework and conventional control respectively

4. CONCLUSION

The proposed framework is the first discussed approach that can detect occurrences of reflective glare from adjacent surfaces and accordingly operate dynamic shading. Although it leads to significantly lower opened shades portions, compromising daylight harvesting potential, it can protect the building's occupants from extreme luminance sources that can lead to discomfort or disability glare. The potential of the new framework is presented through its implementation on a BMS system using a preliminary luminance detection threshold of 30,000 cd/m^2. In that scope, the authors are planning experiments with human subjects to obtain more conclusive thresholds that can effectively balance glare protection with daylight availability. The latter can be either based on absolute luminance values, or also take into account the adaptation level, with the aid of metrics such as background or average luminance of the visual field, while can also be related to the size of the occurring reflections.

ACKNOWLEDGEMENT

REFERENCES

Atzeri, A. M., Cappelletti, F., Tzempelikos, A., & Gasparella, A. (2016). Comfort metrics for an integrated evaluation of buildings performance. *Energy and Buildings 127*, 411-424.

Chan, Y.-C., Tzempelikos, A., Konstantzos, I. (2015). A systematic method for selecting roller shade properties for glare protection. *Energy and Buildings 92*, 81-94.

Geisler-Moroder, D., Lee, E. S., & Ward, G. J. (2016). Validation of the Five-Phase Method for Simulating Complex Fenestration Systems with Radiance against Field Measurements. Lawrence Berkeley National Lab.(LBNL), Berkeley, CA (United States).

Goovaerts, C., Descamps, F. & Jacobs, V. A. (2017). Shading control strategy to avoid visual discomfort by using a low-cost camera: Afield study of two cases. *Building and Environment 125,* 26-38.

Hirning, M., Isoardi G., Cowling I. (2014). Discomfort glare in open plan green buildings. *Energy and Buildings 70*, 427-440.

Jakubiec, J.A., Reinhart, C.F. (2015). A concept for predicting occupants' long term visual comfort within daylit spaces. *Leukos 2724*, 1-18.

Jakubiec, J.A., Reinhart, C.F. (2012). The 'adaptive zone' – a concept for assessing discomfort glare throughout daylit spaces. *Lighting Research and Technology 44*(2), 149-170.

Inanici, M. N. (2006). Evaluation of high dynamic range photography as a luminance data acquisition system. *Lighting Research & Technology, 38*(2), 123-134.

Karlsen, L., Heiselberg, P., Bryn, I., Johra, H. (2015). Verification of simple illuminance based measures for indication of discomfort glare from windows. *Building and Environment 92*, 615-626.

Konis, K. (2013). Evaluating daylighting effectiveness and occupant visual comfort in a side-lit open-plan office building in San Francisco, California. *Building and Environment 59*, 662-677.

Konis, K. (2014). Predicting visual comfort in side-lit open-plan core zones: results of a field study pairing high dynamic range images with subjective responses, *Energy and Buildings 77*, 67-79.

Konstantzos, I., Chan, Y-C., Seibold, J., Tzempelikos, A., Proctor, R.W., Protzman, B. (2015a). View Clarity Index: a new metric to evaluate clarity of view through window shades. *Building and Environment,* pp.206-214.

Konstantzos, I., Tzempelikos, A., Chan, Y-C. (2015b). Experimental and simulation analysis of daylight glare probability in offices with dynamic window shades. *Building and Environment 87*, 244-254.

Konstantzos, I., & Tzempelikos, A. (2017). Daylight glare evaluation with the sun in the field of view through window shades. *Building and Environment 113*, 65-77.

Konstantzos, I., Kim, M., & Tzempelikos, A. (2018). An integrated method and web tool to assess visual environment in spaces with window shades. *Science and Technology for the Built Environment*, 1-13.

Park, B. C., Choi, A. S., Jeong, J. W., & Lee, E. S. (2011). Performance of integrated systems of automated roller shade systems and daylight responsive dimming systems. *Building and Environment 46*(3), 747-757.

Reinhart, C., Doyle, S., Jakubiec, J. A., & Rashida, M. (2017). Glare analysis of daylit spaces: recommendations for practice. http://web.mit.edu/tito_/www/Projects/Glare/GlareRecommendationsForPractice.html (last accessed: May 2018)

Sadeghi, S.A., Karava, P., Konstantzos, I., Tzempelikos, A. (2015). Occupant interactions with shading and lighting systems using different control interfaces: A pilot study. *Building and Environment 97*,177-195.

Scaramuzza, D., Martinelli, A., & Siegwart, R. (2006). A toolbox for easily calibrating omnidirectional cameras. *Intelligent Robots and Systems, IEEE/RSJ International Conference*, 5695-5701

Shen, H., & Tzempelikos, A. (2017). Daylight-linked synchronized shading operation using simplified model-based control. *Energy and Buildings 145*, 200-212.

Singh, R., Lazarus, I. J., & Kishore, V. V. N. (2015). Effect of internal woven roller shade and glazing on the energy and daylighting performances of an office building in the cold climate of Shillong. *Applied energy 159*, 317-333.

Stumpfel, J., Tchou, C., Jones, A., Hawkins, T., Wenger, A., & Debevec, P. (2004). Direct HDR capture of the sun and sky. *Proceedings of the 3rd international conference on Computer graphics, virtual reality, visualisation and interaction in Africa*, 145-149

Suk, Y.S., Schiler, M., Kensek, K. (2016). Is Exterior Glare Problematic?: Investigation on Visual Discomfort Caused by Reflected Sunlight on Specular Building Facades. *PLEA 2016 36th International Conference on Passive and Low Energy Architecture. Cities, Buildings, People: Towards Regenerative Environments,* Los Angeles

Tzempelikos, A., & Athienitis, A. K. (2007). The impact of shading design and control on building cooling and lighting demand. *Solar energy 81*(3), 369-382.

Tzempelikos, A. (2017). Advances on daylighting and visual comfort research. *Building and Environment 113*, 1-4.

Van Den Wymelenberg, K., Inanici, M., (2014). A critical investigation of common lighting design metrics for predicting human visual comfort in offices with daylight. *Leukos 10*(3), 145-164.

Van Den Wymelenberg K., Inanici, M, Johnson P, (2010). The Effect of luminance distribution patterns on occupant preference in a daylit office environment. *Leukos. 7*(2), 103-122

Ward, G. J. (1994). The RADIANCE lighting simulation and rendering system. *Proceedings of the 21st annual conference on Computer graphics and interactive techniques*, 459-472

Ward G. Anyhere Software. HDRgen. http://www.anyhere.com. Last accessed May 2018

Wienold J., Christoffersen J. (2006). Evaluation methods and development of a new glare prediction model for daylight environments with the use of CCD cameras. *Energy and Buildings 38*, 743-757.

Wienold J. (2007). Dynamic simulation of blind control strategies for visual comfort and energy balance analysis. *Proc. of IBPSA 2007 Conference*, Beijing, 1197-1204.

Wienold J. (2009). Dynamic daylight glare evaluation. *Proceedings of IBPSA 2009 conference*, Glascow, Scotland, 944-951.

Wienold J. (2017). EvalGlare Version 2.02.

Yao, J. (2014). An investigation into the impact of movable solar shades on energy, indoor thermal and visual comfort improvements. *Building and environment 71*, 24-32.